

Article

Numerical Study on Aerodynamic Noise Reduction of Pantograph

Fangcheng Shi ¹, Fushan Shi ¹, Xudong Tian ² and Tiantian Wang ^{1,2,*} ¹ College of Mechanical and Vehicle Engineering, Hunan University, Changsha 410082, China² School of Traffic and Transportation Engineering, Central South University, Changsha 410075, China

* Correspondence: wangtiantian@csu.edu.cn

Abstract: A hybrid method incorporating the simulations of noise sources with delayed detached eddy simulation (DDES) and calculations of far-field noise with the Ffowcs Williams–Hawkings (FW-H) equation is used to study the suppression technique for the aerodynamic noise of a Faiveley CX-PG pantograph. Considering that China’s Fuxing bullet trains operate at 350 km/h, the inflow velocity of 350 km/h is applied in this paper. The noise radiated from the panhead area, middle area, and bottom area at an inflow velocity of 350 km/h is distinguished. The noise intensities at the standard observer show that the noise radiated from the panhead area is the strongest, and the sound pressure level spectrum value is larger than the other two in the range above 500 Hz. The influence of applying the wavy rods and modifying the contact strip shape on the aerodynamic noise is discussed in detail. By comparing the acoustic source distribution and the far-field noise intensity, it is found that applying the wavy rods can effectively reduce the panhead noise, especially around the peak frequency. Modifying the shape of the contact strip to a hexagon can suppress the vortex shedding, leading to a lower surface pressure level. Combining the strip modification and wavy rods, the total noise intensity can be diminished by about 3.0 dB.



Citation: Shi, F.; Shi, F.; Tian, X.; Wang, T. Numerical Study on Aerodynamic Noise Reduction of Pantograph. *Appl. Sci.* **2022**, *12*, 10720. <https://doi.org/10.3390/app122110720>

Academic Editor: Yoshinobu Kajikawa

Received: 20 September 2022

Accepted: 19 October 2022

Published: 22 October 2022

Publisher’s Note: MDPI stays neutral with regard to jurisdictional claims in published maps and institutional affiliations.



Copyright: © 2022 by the authors. Licensee MDPI, Basel, Switzerland. This article is an open access article distributed under the terms and conditions of the Creative Commons Attribution (CC BY) license (<https://creativecommons.org/licenses/by/4.0/>).

Keywords: aerodynamic noise; noise suppression; hybrid method; pantograph

1. Introduction

Aerodynamic noise and rolling noise are the two prominent noises radiating from high-speed trains [1]. The sound power of aerodynamic noise increases with flow speed U at a rate of U^6 – U^8 [2,3], while the sound power of rolling noise increases at a rate of three power of the train speed [4]. With the increase of train speed, the proportion of aerodynamic noise in the overall noise gradually increases. When the train speed reaches or exceeds 300 km/h, aerodynamic noise will become predominant in the train noise [5]. In order to alleviate the adverse effects of high-speed train noise on the surrounding environment and passenger comfort, it is necessary to develop aerodynamic noise suppression technique.

The aerodynamic noise of high-speed trains includes a variety of noise sources, and the noise strength is related to the shape of the train and the structure of its components. In particular, the pantograph noise is a key component of the aerodynamic noise of high-speed trains [1,5,6]. Considering that the pantograph is located on the top of the train, the conventional noise barrier for the train body noise cannot effectively reduce the pantograph noise because of the low height [4]. Some studies have been carried out on the pantograph noise based on vehicle tests, wind tunnel experiments, and numerical simulations. Ikeda and Takaishi [7] studied the Aeolian tone suppression mechanism of a perforated pantograph horn and found that the Aeolian tone intensity can be reduced by the periodic holes. By applying porous materials to cover the pantograph surface, Sueki et al. [8] confirmed that the porous materials could decrease the pantograph noise. Kurita et al. [9] developed more effective shape of noise insulation plates to design low-noise pantographs, of which the noise level can be diminished by more than 2 dB. Recently, Guo et al. [10] studied three

aerodynamic noise reduction measures of opening, slotting, and airfoil. The results show that the open arms and the airfoil bow head can reduce the aerodynamic noise to over 1.0 dBA.

The pantograph noise generation is mainly due to vortex shedding around the rods of the pantograph (such as the arm frame and the contact strip), which has been quite well understood [11]. Aiming to delay flow separation and weaken vortex shedding strength, some active means and passive approaches have been developed, such as introducing plasma actuator [12], adding bio-inspired serrations [13] or cables [14]. Recently, the wavy rod has attracted the attention of researchers, and a series of studies have been performed. Zhang et al. [15] studied the three-dimensional vortex characteristics behind the wavy cylinders at a subcritical Reynolds number and found that the boundary layer separation is delayed markedly with increasing wave amplitude. Bai et al. [16] investigated the influence of wavelength and wave amplitude on the capability of noise suppression. It is observed that the wavy cylinder with optimum wavelength and wave amplitude can reduce the peak value of sound pressure level up to 36.7 dB. Chen et al. [17] studied the noise control mechanisms with the wavy cylinder at different Reynolds numbers, and it was found that the boundary vorticity flux and boundary enstrophy flux are also remarkably weakened.

Basically, the previous research about the wavy rod mainly focused on the noise radiated from a cylinder. Nevertheless, the pantograph consists of many parts, which considerably complicates the composite noises. Meanwhile, the surface of the wavy rod also impacts the pantograph noise, which is insufficiently considered. In this paper, we apply the wavy rod to the pantograph and analyze the influence of the wavy surface on the pantograph noise. Additionally, the contact strip shape modification is conducted to study the suppression of the pantograph noise.

As for the organization of this paper, we first introduce the geometry of the pantograph and the grid. Then, the computational methods are described in Section 3. Next, the simulation results are presented, including the flowfield and the far-field noise. The influence of wavy rods and contact strip modification on the acoustic sources and noise are discussed. Conclusions are summarized in the final section.

2. Geometry Description

The research object is a Faiveley CX-PG pantograph, and the configuration is shown in Figure 1a. It can be classified into three areas: the panhead area, middle area, and bottom area. These three areas are identified by different colors in Figure 1a. The rods on the panhead and middle areas play an important part in generating the aerodynamic noise by inducing the separation flow and the vortex shedding. In order to study the capability of the sinusoidal wavy rod to reduce aerodynamic noise, the noise radiated from a pantograph of the wavy surface is simulated and analyzed. Figure 1b shows the configuration of the wavy rod model. The diameter of the wavy rod D is a function of the spanwise coordinate z , and it is given by

$$D(z) = D_{\text{ori}} - 0.1D_{\text{ori}} \cdot \cos\left(2\pi \frac{z}{5D_{\text{ori}}}\right) \quad (1)$$

where $D_{\text{ori}}(z)$ is the diameter of the original model. According to the previous study [16], the optimum wavelength of about $5D_{\text{ori}}$ can reduce the noise of the cylinder the most. Hence, the wavelength of $5D_{\text{ori}}$ is applied in Equation (1). Moreover, the optimization design of the contact strip is considered to reduce the pantograph noise further. As shown in Figure 1c, the leading and trailing edges of the rectangular contact strip are modified into an equilateral triangle to weaken the vortex shedding.

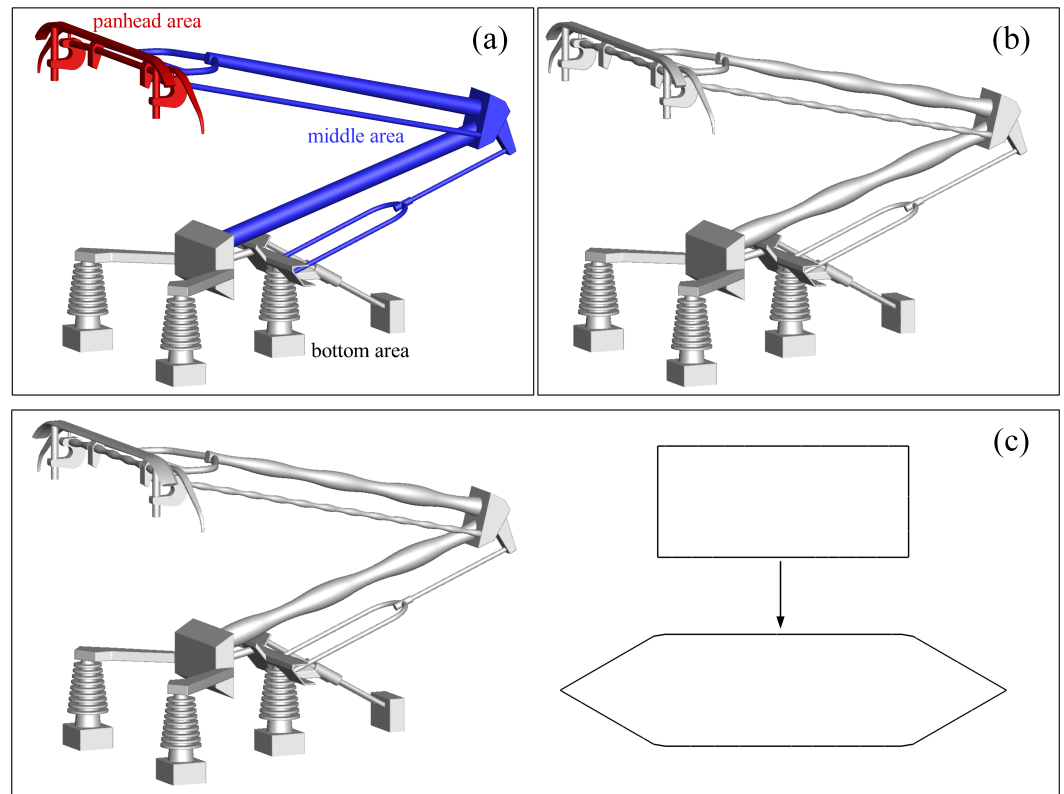


Figure 1. Schematic diagram of the three pantograph models: (a) original model; (b) wavy rod model; (c) hexagonal strip model.

The flow of 350 km/h is simulated and the freestream conditions are listed in Table 1. Figure 2 shows the computational domain used in this study. The size of the domain is $50 \times 15 \times 7.5$ m, and the pantograph model is located laterally symmetrically at about 15 m downstream of the inlet. The boundary conditions of the computational domain are given in Table 2.

Table 1. Details of the freestream conditions.

U_∞ (km/h)	ρ_∞ (kg/m ³)	T_∞ (K)
350	1.225	288.15

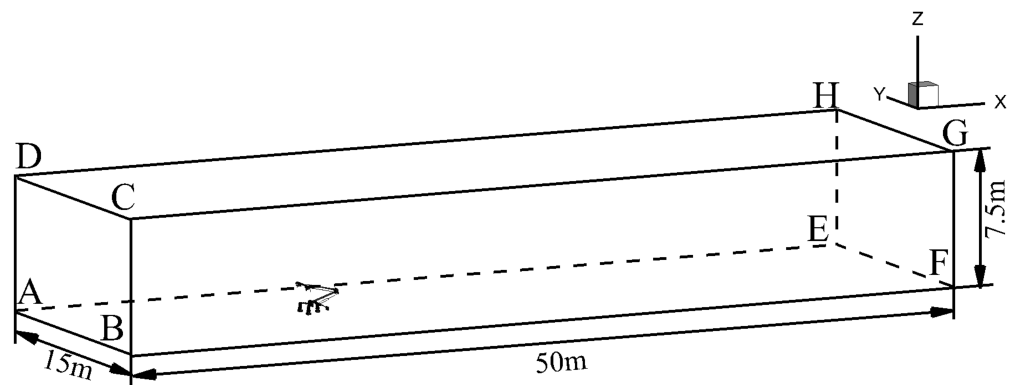


Figure 2. Computational domain.

Table 2. Boundary conditions of the computational domain.

Velocity Inlet	Symmetry	Pressure Outlet	Wall
Face ABCD	Face AEHD, BFGC, CGHD	Face EFGH	Face ABFE

The unstructured grid applied for the current simulations is displayed in Figure 3. The pantograph surface is divided into the triangular mesh with a grid scale of (3–5) mm to capture the structure. The grid is clustered in the near pantograph surface, and the thickness of the first layer of the boundary layer is 5×10^{-6} m. Figure 4 presents the distribution of y^+ , which indicates that it is close to 1, and the average value equals 0.47. The total grid number is approximately 35 million. By reducing the grid size near the pantograph, a finer grid of 43 million cells has been applied to verify grid independence.

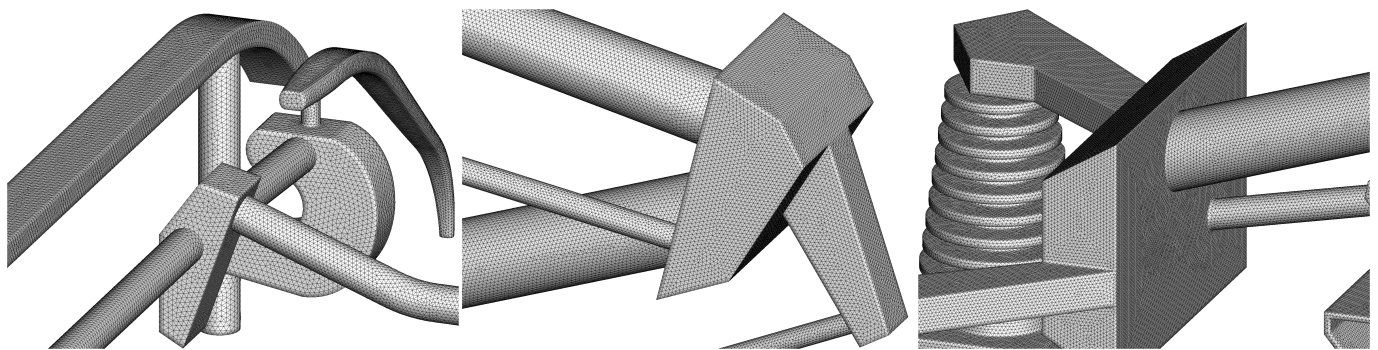


Figure 3. Computational grid on the pantograph surface.

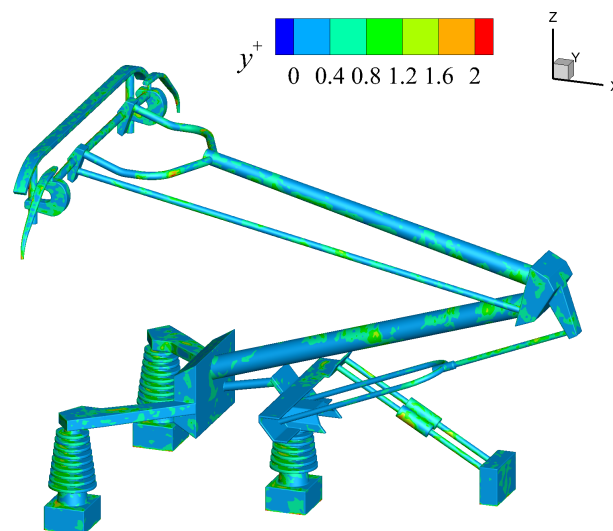


Figure 4. Distribution of y^+ on the pantograph surface.

3. Computational Methods

3.1. Delay Detached Eddy Simulation

Delayed detached eddy simulation (DDES) has been widely used in turbulence and aeroacoustic simulations [18–20], which is employed to compute the flowfield and the acoustic source in this paper. The current DDES simulations are based on the Realizable $k - \epsilon$ model, written as follows [21]:

$$\begin{cases} \frac{\partial \rho k}{\partial t} + \frac{\partial \rho k u_j}{\partial x_j} = \frac{\partial}{\partial x_j} \left[\left(\mu + \frac{\mu_t}{\sigma_k} \right) \frac{\partial k}{\partial x_j} \right] + \mu_t S^2 - \frac{\rho k^{1.5}}{l_{DDES}} - 2\rho \epsilon M_t^2 \\ \frac{\partial \rho \epsilon}{\partial t} + \frac{\partial \rho \epsilon u_j}{\partial x_j} = \frac{\partial}{\partial x_j} \left[\left(\mu + \frac{\mu_t}{\sigma_\epsilon} \right) \frac{\partial \epsilon}{\partial x_j} \right] + C_1 \rho S \epsilon - C_2 \rho \frac{\epsilon^2}{k + \sqrt{\nu \epsilon}} \end{cases} \quad (2)$$

where M_t is the turbulent Mach number. The model constants C_2 , σ_k , and σ_ϵ are 1.9, 1.0, and 1.2, respectively. The quantity C_1 is computed from

$$C_1 = \max\left(0.43, \frac{\eta}{\eta + 5}\right), \eta = S \frac{k}{\epsilon}, S = \sqrt{2S_{ij}S_{ij}} \tag{3}$$

The length scale l_{DDES} is defined as

$$l_{\text{DDES}} = l_{Rk\epsilon} - f_d \max(0, l_{Rk\epsilon} - l_{\text{LES}}), l_{Rk\epsilon} = \frac{k^{1.5}}{\epsilon}, l_{\text{LES}} = C_{\text{DDES}} \Delta_{\text{max}} \tag{4}$$

where the constant C_{DDES} equals 0.61. Δ_{max} is the maximum grid spacing, $\Delta_{\text{max}} = \max(\Delta_x, \Delta_y, \Delta_z)$. The shielding function f_d is given by

$$f_d = 1 - \tanh\left[(20r_d)^3\right], r_d = \frac{v_t + \nu}{\sqrt{U_{i,j}U_{i,j}}\kappa^2 d^2}, \kappa = 0.41 \tag{5}$$

The equations are solved using ANSYS fluent. With respect to the numerical methods, the Roe scheme is used for the convective flux, and the second-order discretization is applied for the flow equations and the turbulence transport equations. The time advancement is performed with a second-order time integration scheme. The time step $\Delta t = 5 \times 10^{-5}$ s is used in the simulations, and 4000 time steps are calculated to obtain the acoustic source information.

3.2. Ffowcs Williams–Hawkings Equation

Considering the high computational cost of noise propagation, the far-field noise evaluation is performed using the Ffowcs Williams–Hawkings (FW-H) equation [22]. In this work, the pantograph surface is defined as the FW-H surface. Since the flow is low subsonic, the contribution of the Lighthill stress tensor is small, and the volume integral of the FW-H equation is omitted. Thus, the sound pressure at the far-field can be written as the sum of thickness term and loading term:

$$p'(\mathbf{x}, t) = p'_T(\mathbf{x}, t) + p'_L(\mathbf{x}, t) \tag{6}$$

where

$$4\pi p'_T(\mathbf{x}, t) = \int_{f=0} \left[\frac{\rho_a U_i n_i}{r(1-M_r)^2} + \frac{\rho_a U_n \frac{r_i}{r} M_i}{r(1-M_r)^3} \right]_{\tau=\tau_e} dS + \int_{f=0} \left[\frac{\rho_a U_n c_a (M_r - M^2)}{r^2(1-M_r)^3} \right]_{\tau=\tau_e} dS \tag{7}$$

$$4\pi p'_L(\mathbf{x}, t) = \int_{f=0} \left[\frac{L_i \frac{r_i}{r}}{c_a r(1-M_r)^2} + \frac{L_i \frac{r_i}{r} \cdot \frac{r_i}{r} M_i}{c_a r(1-M_r)^3} \right]_{\tau=\tau_e} dS + \int_{f=0} \left[\frac{L_i \frac{r_i}{r} \cdot (M_r - M^2)}{r^2(1-M_r)^3} + \frac{L_i \frac{r_i}{r} - L_i M_i}{r^2(1-M_r)^2} \right]_{\tau=\tau_e} dS \tag{8}$$

The subscript a denotes the quantities of the surrounding medium. The surface $f = 0$ corresponds to the source surface. r and r_i represent the magnitude and the direction of the vector from the source surface to the observer \mathbf{x} , respectively. The quantities U_i , M_i , M_r , and L_i are given by

$$\begin{cases} U_i = \left(1 - \frac{\rho}{\rho_a}\right)v_i + \frac{\rho u_i}{\rho_a} \\ M_i = \frac{v_i}{c_a} \\ M_r = M_i \frac{r_i}{r} \\ L_i = (p' \delta_{ij} - \sigma_{ij})n_j + \rho u_i u_n \end{cases} \tag{9}$$

In order to take into account that the sound reflects on the ground, an additional observer is arranged in the mirror position. The sound pressure at the two observer points is calculated by Equations (6)–(8), and the obtained time-domain signals are superimposed to obtain the sound pressure with considering the ground effect.

3.3. Numerical Validation

A simulation of cylinder noise is conducted to verify the hybrid method of simulating noise by combining DDES with the FW-H equation. The diameter of the cylinder is $D = 19$ mm. The inflow velocity is 69.19 m/s, and the Reynolds number based on the diameter is approximately 90,000. The free-stream condition is similar to that in Refs. [19,23]. The grid is clustered in the cylinder surface, and the value of y^+ is close to 1.

Figure 5 shows the instantaneous contour of spanwise vorticity. The boundary layer separates at the lateral sides of the cylinder and generates the shear layer, which rolls up to form the vortex street structure. The vortex shedding causes unsteady force and generates aerodynamic noise. A standard observer is arranged at $(0, 128D, 0)$. Table 3 compares the maximum value of sound pressure level SPL_{max} and corresponding Strouhal number St_p . It indicates that the present hybrid method can simulate the noise intensity and capture the dominant frequency.

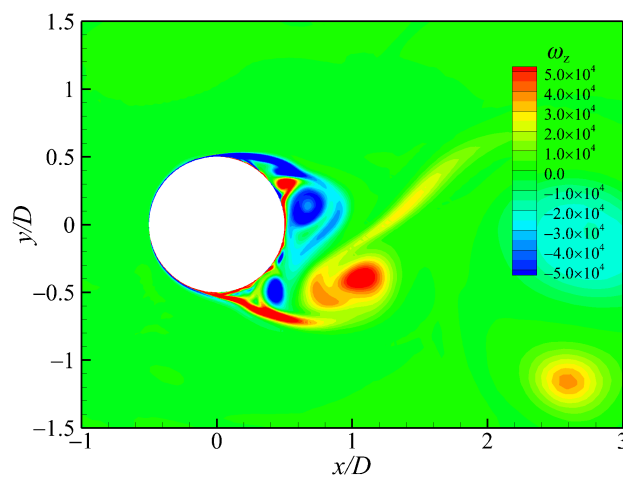


Figure 5. Instantaneous contour of spanwise vorticity ω_z .

Table 3. Comparison between the present and previous results.

	Present	Tan et al. [19]	Li et al. [23]
SPL_{max}	99.61	100.67	98.76
St_p	0.194	0.201	0.179

4. Results and Discussion

4.1. Flowfield and Acoustic Source of the Original Model

Turbulent eddies are an important flow structure for the noise generation. They evolve gradually along the flow direction. Figure 6 provides the instantaneous iso-surface of the Q -criterion, which is colored by the velocity magnitude. As can be seen, eddies generated by the panhead are small and they are elongated in the x direction when flowing downstream. The air flowing through the bottom area of the pantograph produces the large-scale eddies, of which the position increases as they flow downstream. The large-scale eddies merge with eddies in the wake of the middle area and the panhead area.

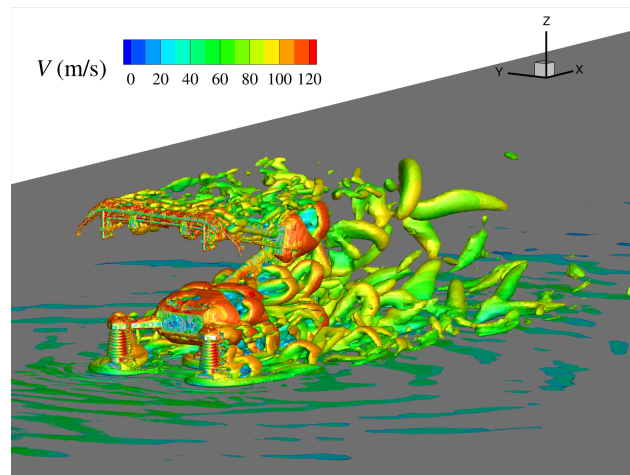


Figure 6. Instantaneous snapshot of eddies extracted by the Q -criterion ($Q = 10^4 \text{s}^{-2}$) and colored by the velocity magnitude.

Figure 7 demonstrates the instantaneous contour of the pressure fluctuation, which is non-dimensionalized by the freestream pressure. The noise radiated from the panhead area of the pantograph is transparent, and the wave front is approximately circular and the directivity is nearly uniform. The middle and bottom areas also radiate out noise, but the noise amplitude is too low to be distinguishable. In the downstream of the pantograph, eddies in the wake lead to the hydrodynamic pressure fluctuations propagating downstream rather than the sound wave.

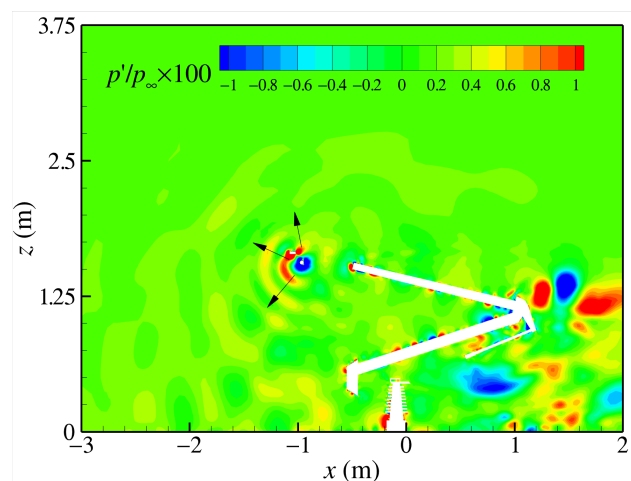


Figure 7. Instantaneous contour of the non-dimensionalized pressure fluctuation $p'/p_\infty \times 100$ on the symmetric surface ($y = 0$).

Based on the time history of the surface pressure, the dimensional power spectral density (PSD) values of the pressure time derivative can be calculated. Then, the surface pressure level (SPL) for the 1/3 octaves f_c is provided as follows:

$$\text{SPL}(f_c) = 10 \cdot \log_{10} \frac{\text{PSD}(f_c)}{p_{\text{ref}}^2}, p_{\text{ref}} = 2 \times 10^{-5} \text{Pa} \quad (10)$$

The contour of SPL on the pantograph surface at different frequencies is displayed in Figure 8. It indicates that the acoustic source of high-frequency noise is mainly concentrated in the panhead area, while the low-frequency noise is radiated from the middle and bottom areas of the pantograph. This acoustic source distribution is consistent with the eddy scales illustrated in Figure 6.

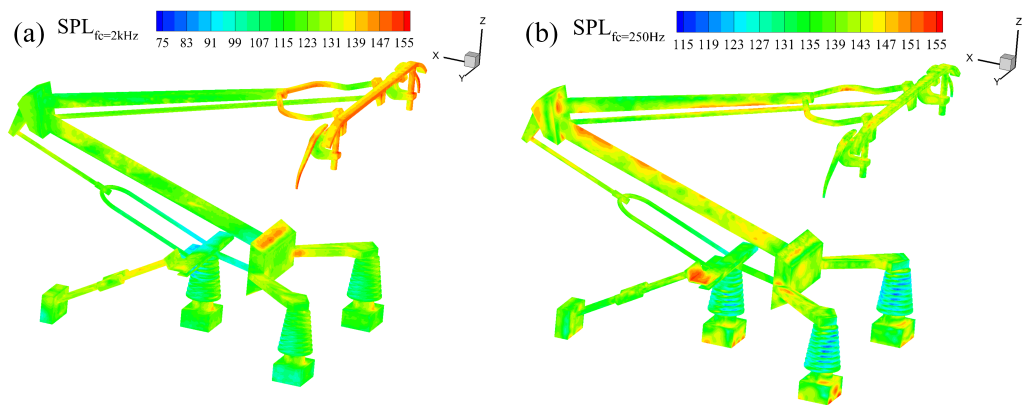


Figure 8. Contour of the surface pressure level on the pantograph surface: (a) $f_c = 2$ kHz; (b) $f_c = 250$ Hz.

4.2. Far-Field Noise of the Original Model

In order to study the far-field noise radiated from the original model, a standard observer point is selected, and its coordinates are (0, 25, 3.5) m. The time history of the sound wave is divided into three parts, namely the noise radiated from the panhead, middle, and bottom areas. Figure 9 compares the overall sound pressure level (OASPL) of the noise radiated from different parts, and the OASPL values are 105.12 dB, 103.29 dB, 94.61 dB, and 98.87 dB, respectively. It is found that the noise intensity of the panhead area is obviously higher than the other two parts, which is consistent with the qualitative analysis based on the pressure fluctuation contour shown in Figure 7. In addition, the far-field noise is also calculated using a finer grid of 43 million cells. The OASPL value of the noise radiated from all parts is 104.99 dB, indicating that the grid independence is well satisfied.

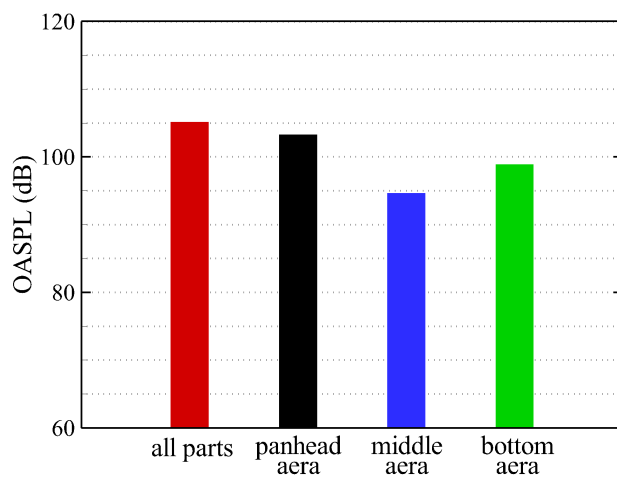


Figure 9. Comparisons of overall sound pressure level between different noise parts.

Furthermore, the A-weighted sound pressure level spectra (A-weighted SPL) of noise radiated from different parts are presented in Figure 10. The peak frequency f_p of the total noise is 630 Hz, and the characteristic length scale L according to Aeolian tone characteristic is

$$L = \frac{StU_\infty}{f_p} = \frac{0.2 \times 350/3.6}{630} = 0.031 \text{ m} \tag{11}$$

The value is close to the result in Ref. [24]. By comparing the contribution of different parts to the total noise, it is found that the noise radiated from the middle area is close to that of the bottom area, apart from the peak frequency of the former being lower than that of the

latter. In the high-frequency range ($f > f_p$), the spectrum value of noise radiated from the panhead area is larger than the noise radiated from the middle and bottom areas. However, the noise radiated from the panhead area is weaker than that from the other two parts in the low-frequency range ($f < f_p$).

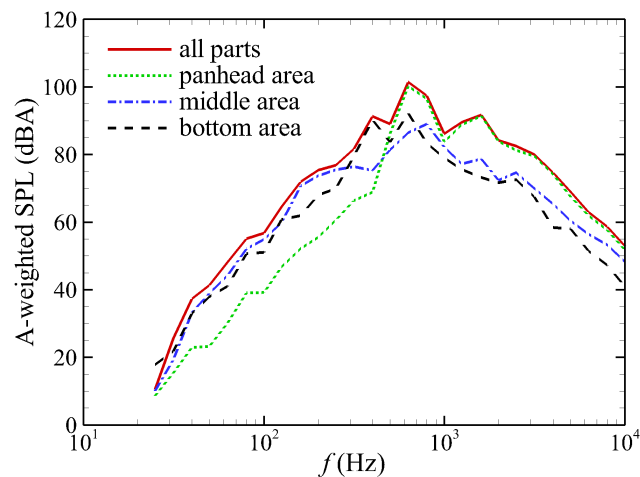


Figure 10. A-weighted sound pressure level spectra of noise radiated from different parts of the pantograph.

4.3. Influence of Wavy Rods on the Aerodynamic Noise

According to the previous research [15], the boundary layer separation of the wavy cylinder is markedly delayed and the noise intensity can be suppressed. In order to study the influence of wavy rods on the aerodynamic noise of the pantograph, the surface pressure level is firstly compared in Figure 11. Through modifying the cross bar surface, the value of the pressure time derivative is obviously decreased, as marked by an ellipse. Applying the wavy rods can also reduce the acoustic source in the middle area, but the reduction magnitude is relatively small, such as in the lower arm frame.

Next, the values of OASPL at the standard observer are quantitatively compared in Figure 12. The components of the bottom area remain the same, so the corresponding noise intensity is not displayed. As shown in Figure 12, the noise generated by the middle area of the wavy rod model is slightly weaker than that of the original model, and the difference is about 0.6 dB. Then, we focus on the noise radiated from the panhead area of the two models. The difference between the two models is 2.4 dB, and the results suggest that applying the wavy rods can diminish the panhead noise intensity. Furthermore, the change of A-weighted SPL at different frequency ranges is studied. The data in Figure 13 reveals that the panhead noise suppression is mainly concentrated around the peak frequency, from 560 Hz to 3600 Hz. Nevertheless, the noise intensity in the higher frequency range ($f > 3600$ Hz) is strengthened.

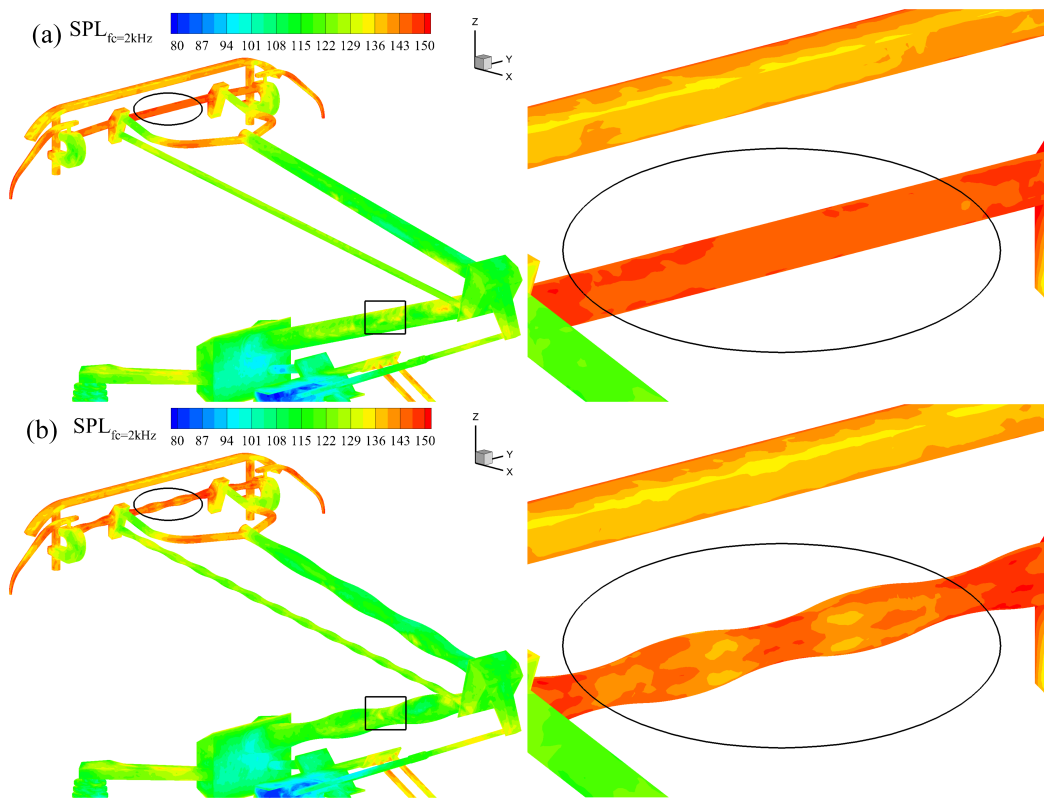


Figure 11. Contour of the surface pressure level at $f_c = 2$ kHz: (a) original model; (b) wavy rod model.

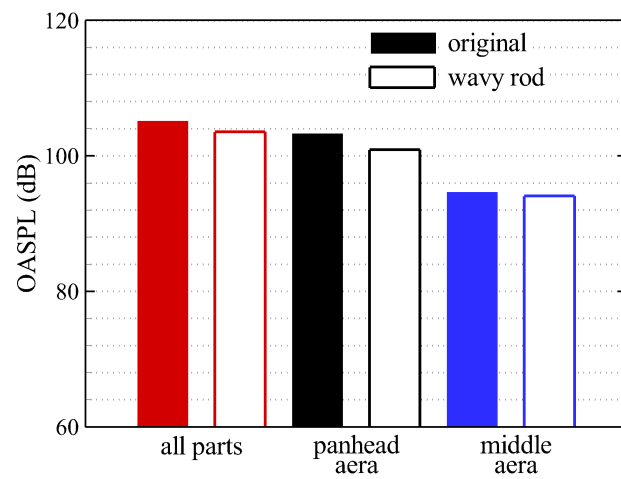


Figure 12. Comparison of overall sound pressure level between the original model and wavy rod model.

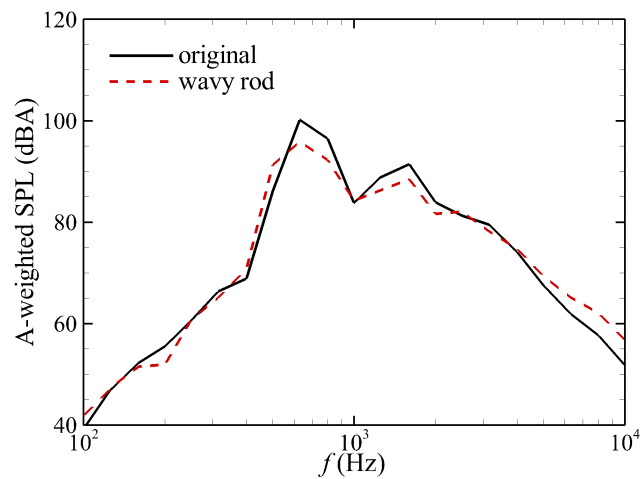


Figure 13. A-weighted sound pressure level spectra of noise radiated from the panhead of the original model and wavy rod model.

4.4. Influence of Contact Strip Modification on the Aerodynamic Noise

Apart from the cross bar, the contact strip plays a key role in the panhead noise. The rectangular contact strip of the original model can induce strong vortex shedding, resulting in a high level of turbulent kinetic energy (TKE), as depicted in Figure 14. To weaken the vortex shedding, we modify the shape of the contact strip to a hexagon. The distribution of TKE reveals that the unsteady flow around the trip is suppressed. Figure 15 shows the surface pressure level of the hexagonal strip model, and it can be found that the pressure time derivative of the contact strip is decreased, which means that the sound wave generated by the contact strip is alleviated.

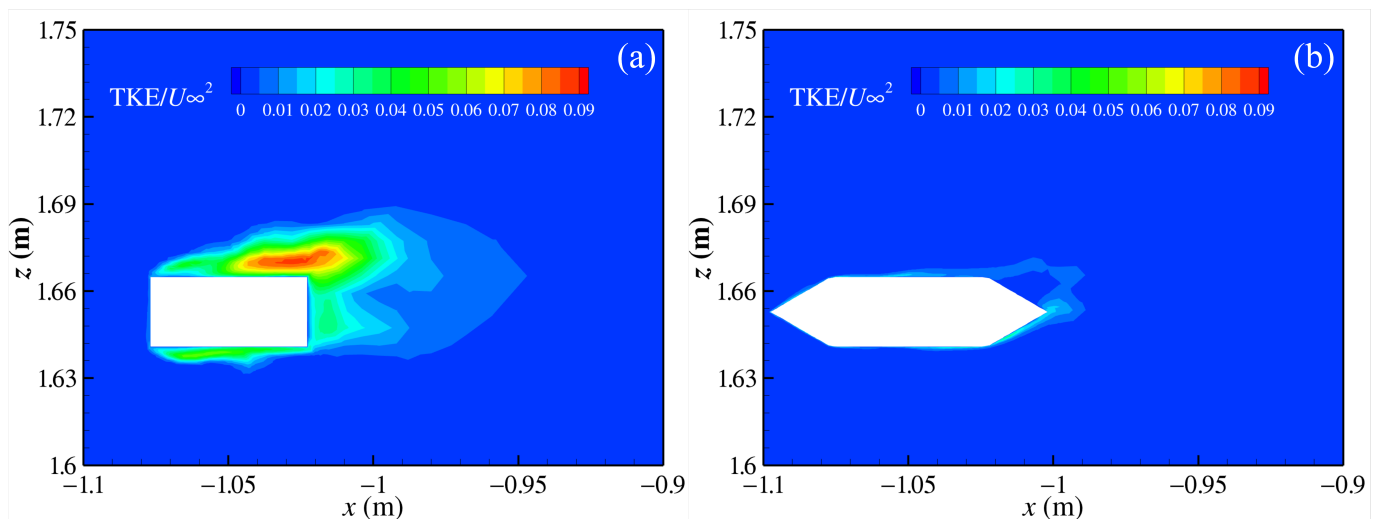


Figure 14. Contour of non-dimensionalized turbulent kinetic energy (TKE): (a) original model; (b) hexagonal strip model.

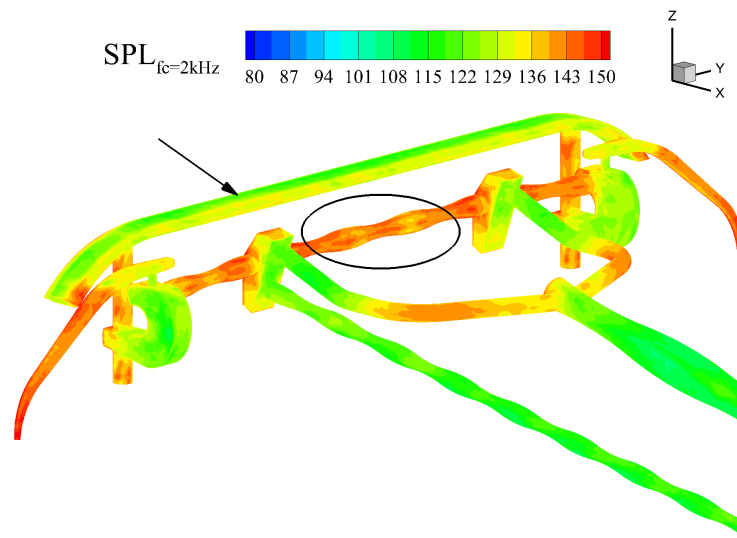


Figure 15. Contour of the surface pressure level at $f_c = 2$ kHz of the hexagonal strip model.

Then, the OASPL value at the standard observer is calculated, and Figure 16 presents the values of the original model and hexagonal strip model. The OASPL values of noise radiated from the panhead and middle areas of the hexagonal strip model are 97.77 dB and 93.95 dB, respectively, which suggests that modifying the contact strip can further decrease the panhead noise intensity up to 5.52 dB. The OASPL value of total noise is reduced from 105.12 dB to 102.18 dB accordingly. Moreover, Figure 17 compares the A-weighted SPL between the wavy rod model and the hexagonal strip model. It is evident that the noise intensity in the high-frequency range ($f > 500$ Hz) is all weakened, which is consistent with the surface pressure level reduction at $f_c = 2$ kHz given in Figure 15. In addition, the value of A-weighted SPL at $f = 315$ Hz is increased slightly.

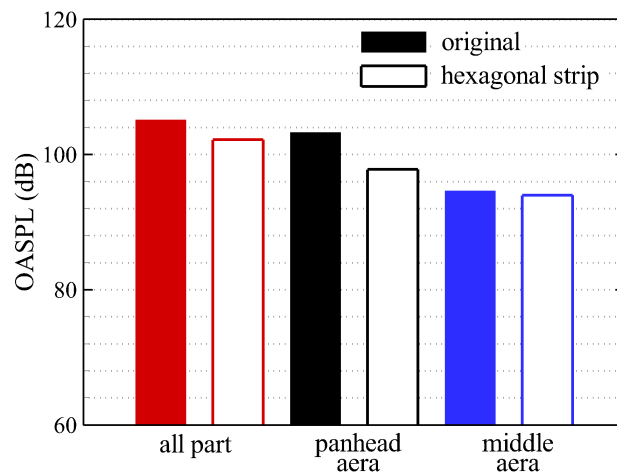


Figure 16. Comparison of the overall sound pressure level between the original model and hexagonal strip model.

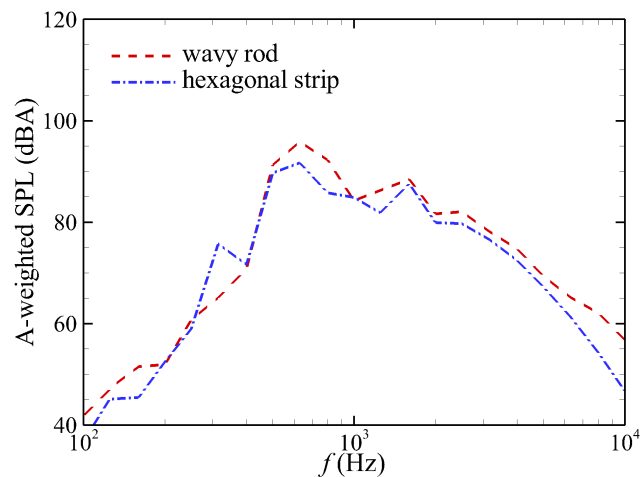


Figure 17. A-weighted sound pressure level spectra of noise radiated from the panhead of the wavy rod model and hexagonal strip model.

5. Conclusions

In this paper, we studied the feasibility of applying the wavy rods to reduce the aerodynamic noise of a Faiveley CX-PG pantograph based on a hybrid method. The influence of contact strip modification on aerodynamic noise was also studied. The effect of the above noise suppression techniques on the acoustic source intensity and the noise magnitude at different frequencies was explored in detail. The main conclusions drawn in this work are as follows:

1. The panhead area is a primary acoustic source, of which the noise is stronger than that of the middle and bottom areas at an inflow velocity of 350 km/h. The sound energy of the panhead noise is concentrated in the high-frequency range ($f > 500$ Hz).
2. Applying the wavy rods to change the cross bar surface can effectively reduce the panhead noise, especially the sound energy around the peak frequency. However, changing the arm surface has little effect on weakening the noise radiated out from the middle area.
3. Modifying the shape of the contact strip to a hexagon can suppress the vortex shedding and decrease the surface pressure level. By combining the modification of the strip shape and the application of the wavy rods, the panhead noise intensity can be diminished by 5.52 dB.

It can be concluded that applying the wavy rods and modifying the contact strip shape are effective ways to reduce the aerodynamic noise of the pantograph.

Author Contributions: Conceptualization, F.S. (Fangcheng Shi); Formal analysis, F.S. (Fangcheng Shi); Funding acquisition, T.W.; Investigation, F.S. (Fangcheng Shi); Software, X.T.; Visualization, F.S. (Fushan Shi); Writing—original draft, F.S. (Fangcheng Shi). All authors have read and agreed to the published version of the manuscript.

Funding: This research was funded by National Key R & D Program of China Grant No. 2020YFA0710903-C, Fundamental Research Funds for the Central Universities Grant No. 531118010787, the National Natural Science Foundation of China Grant Nos. 51905547 and 52078199, the China National Railway Group Limited Grant No. P2021J036, and the Young Elite Scientists Sponsorship Program by CAST Grant No. 2020QNRC001.

Institutional Review Board Statement: Not applicable.

Informed Consent Statement: Not applicable.

Data Availability Statement: Not applicable.

Acknowledgments: The authors acknowledge the National Key R & D Program of China (Grant No. 2020YFA0710903-C), Fundamental Research Funds for the Central Universities (Grant No. 531118010787), Key Laboratory of Hypersonic Aerodynamic Force and Heat Technology/AVIC Aerodynamics Research Institute Foundation, the National Natural Science Foundation of China (Grant Nos. 51905547 and 52078199), the China National Railway Group Limited (Grant No. P2021J036), and the Young Elite Scientists Sponsorship Program by CAST (Grant No. 2020QNR001). This work was carried out in part using computing resources at the High Performance Computing Center of Central South University.

Conflicts of Interest: The authors declare no conflict of interest.

References

1. Thompson, D.J.; Iglesias, E.L.; Liu, X.; Zhu, J.; Hu, Z. Recent developments in the prediction and control of aerodynamic noise from high-speed trains. *Int. J. Rail Transp.* **2015**, *3*, 119–150. [[CrossRef](#)]
2. Curl, N. The influence of solid boundaries upon aerodynamic sound. *Proc. R. Soc. Lond. Ser. A Math Phys. Sci.* **1955**, *231*, 505–514.
3. Lighthill, M.J. On sound generated aerodynamically. I. General theory. *Proc. R. Soc. Lond. Ser. A Math Phys. Sci.* **1952**, *211*, 564–587.
4. Poisson, F. Railway noise generated by high-speed trains. In *Noise and Vibration Mitigation for Rail Transportation Systems. Notes on Numerical Fluid Mechanics and Multidisciplinary Design*; Anderson, D., Gautier, P., Iida, M., Nelson, J.T., Thompson, D.J., Tielkes, T., Towers, D.A., de Vos, P., Nielsen, J.C.O., Eds.; Springer: Berlin/Heidelberg, Germany, 2015; pp. 457–480.
5. Talotte, C. Aerodynamic noise: A critical survey. *J. Sound Vib.* **2000**, *231*, 549–562. [[CrossRef](#)]
6. Zhang, J.; Guo, T.; Sun, B.; Zhou, S.; Zhao, W. Research on characteristics of aerodynamic noise source for high-speed train. *J. China Railw. Soc.* **2015**, *37*, 10–17. (In Chinese)
7. Ikeda, M.; Takaishi, T. Perforated Pantograph Horn Aeolian Tone Suppression Mechanism. *Q. Rep. RTRI* **2004**, *45*, 169–174. [[CrossRef](#)]
8. Sueki, T.; Ikeda, M.; Takaishi, T. Aerodynamic noise reduction using porous materials and their application to high-speed pantographs. *Q. Rep. RTRI* **2009**, *50*, 26–31. [[CrossRef](#)]
9. Kurita, T.; Hara, M.; Yamada, H.; Wakabayashi, Y.; Mizushima, F.; Satoh, H.; Shikama, T. Reduction of pantograph noise of high-speed trains. *J. Mech. Syst. Transp. Logist.* **2010**, *3*, 63–74. [[CrossRef](#)]
10. Guo, J.; Tan, X.M.; Yang, Z.G.; Xue, Y.Q.; Shen, Y.N.; Wang, H.W. Aeroacoustic optimization design of the middle and upper part of pantograph. *Appl. Sci.* **2022**, *12*, 8704. [[CrossRef](#)]
11. Talotte, C.; Gautier, P.-E.; Thompson, D.J.; Hanson, C. Identification, modelling and reduction potential of railway noise sources: a critical survey. *J. Sound Vib.* **2003**, *267*, 447–468. [[CrossRef](#)]
12. Al-Sadawi, L.; Chong, T.P. Circular cylinder wake and noise control using DBD plasma actuator. In Proceedings of the 25th AIAA/CEAS Aeroacoustics Conference, Delft, The Netherlands, 20–23 May 2019.
13. Shi, L.; Zhang, C.; Wang, J.; Ren, L. Numerical simulation of the effect of bionic serrated structures on the aerodynamic noise of a circular cylinder. *J. Bionic Eng.* **2012**, *9*, 91–98. [[CrossRef](#)]
14. Li, L.; Liu, P.Q.; Xing, Y.; Guo, H. Experimental investigation on the noise reduction method of helical cables for a circular cylinder and tandem cylinders. *Appl. Acoust.* **2019**, *152*, 79–87. [[CrossRef](#)]
15. Zhang, Z.; Tu, J.; Zhang, K.; Yang, H.; Han, Z.; Zhou, D.; Xu, J.; Zhang, M. Vortex characteristics and flow-induced forces of the wavy cylinder at a subcritical Reynolds number. *Ocean Eng.* **2021**, *222*, 108593. [[CrossRef](#)]
16. Bai, H.; Lu, Z.; Wei, R.; Yang, Y.; Liu, Y. Noise reduction of sinusoidal wavy cylinder in subcritical flow regime. *Phys. Fluids* **2021**, *33*, 105120. [[CrossRef](#)]
17. Chen, B.; Yang X.; Chen, G.; Tang, X.; Ding, J.; Weng, P. Numerical study on the flow and noise control mechanism of wavy cylinder. *Phys. Fluids* **2022**, *34*, 036108. [[CrossRef](#)]
18. Spalart, P.R.; Deck, D.; Shur, M.L.; Squires, K.D. A new version of detached-eddy simulation, resistant to ambiguous grid densities. *Theor. Comput. Fluid Dyn.* **2006**, *20*, 181–195. [[CrossRef](#)]
19. Tan, X.M.; Xie, P.P.; Yang, Z.G.; Gao, J.Y. Adaptability of Turbulence Models for Pantograph Aerodynamic noise simulation. *Shock Vib.* **2019**, *2019*, 6405809. [[CrossRef](#)]
20. Wu, Z.; Gao, Z.; Jiang, C.; Lee, C. An in-depth numerical investigation of a supersonic cavity-ramp flow with DDES method. *Aerosp. Sci. Technol.* **2019**, *89*, 253–263. [[CrossRef](#)]
21. ANSYS Fluent Theory Guide, 2020 R1; ANSYS, Inc.: San Jose, CA, USA, 2020.
22. Ffowcs Williams, J.E.; Hawkings, D.L. Sound generation by turbulence and surfaces in arbitrary motion. *Philos. Trans. R. Soc. Lon. Ser. A Math. Phys. Sci.* **1969**, *264*, 321–342.
23. Li, L.; Liu, P.Q.; Xing, Y.; Guo, H.; Tian, Y. Far-field aeroacoustic experimental study of flow around a circular cylinder at subcritical Reynolds number. *J. Beijing Univ. Aeronaut. Astronaut.* **2016**, *42*, 977–983. (In Chinese)
24. Tan, X.M.; Yang, Z.G.; Tan, X.M.; Wu, X.I.; Zhang, J. Vortex structures and aeroacoustic performance of the flow field of the pantograph. *J. Sound Vib.* **2018**, *432*, 17–32.